Tetrahedron 65 (2009) 3980–3989

Contents lists available at ScienceDirect

Tetrahedron

journal homepage: www.elsevier.com/locate/tet

New dicationic derivatives of dibenzotetraaza[14]annulene: tuning DNA-binding properties

Dariusz Pawlica [a], Marijana Radić-Stojković [b], Łukasz Dudek [a], Ivo Piantanida [b], Lesław Sieroń [c], Julita Eilmes [a,*]

[a] Department of Chemistry, Jagiellonian University, Ingardena 3, 30-060 Kraków, Poland
[b] Laboratory for Supramolecular and Nucleoside Chemistry Ruđer Bošković Institute, PO Box 180, HR-10002 Zagreb, Croatia
[c] Institute of General and Ecological Chemistry, Technical University of Łódź, Żeromskiego 116, 90-924 Łódź, Poland

ARTICLE INFO

Article history:
Received 4 December 2008
Received in revised form 20 February 2009
Accepted 12 March 2009
Available online 21 March 2009

Keywords:
Dibenzotetraaza[14]annulene
Synthesis
Crystal structure
DNA binding
UV–vis titration
DNA thermal denaturation
Ethidium bromide displacement

ABSTRACT

Four new water-soluble derivatives of dibenzotetraaza[14]annulene have been synthesized, bearing *meso* substituents with different structures and dimensions: 3-(*N*,*N*,*N*-trimethylammonium)propyl, 3-(*N*-pyridinium-1-yl)propyl, 2-[3-(*N*,*N*,*N*-trimethylammonium)propoxy]benzoyl, and 2-[3-(*N*-pyridinium-1-yl)-propoxy]benzoyl. The crystal structures of 3-(trimethylammonium)propyl and (*N*,*N*,*N*-trimethyl-ammonium)propoxy]benzoyl derivatives were determined by single crystal X-ray analysis. According to the UV–vis titrations, thermal denaturation experiments, and ethidium bromide displacement assays, all compounds presented here interact strongly with double stranded (*ct*)-DNA. The product equipped with 3-(trimethylammonium)propyl pendant groups and two positive charges interacts with DNA in one dominant binding mode, whereas the other three derivatives revealed more complex mixed-type interactions. The results have been discussed in terms of dimensions, geometry, and electronic properties of the evaluated compounds, on the basis of corresponding crystallographic data.

1. Introduction

Interactions between various small molecules and nucleic acids are currently of great interest, due to both their biological significance and their relevance to medical applications.[1] Among the variety of DNA-binders explored so far, the porphyrins belong to those, which have been the most extensively studied.[2] In contrast, little is known about the biological activity of their close structural analogues, dibenzotetraaza[14]annulenes (DBTAAs). We have recently reported the first studies, to our knowledge, of the interactions of dibenzotetraaza[14]annulene derivatives with DNA/RNA as well as screening their antiproliferative activity against human tumor and normal cell lines.[3,4] The results showed that DNA/RNA binding and biological activity were remarkably influenced by the properties of the pendant *meso* substituents. Here, we present the synthesis, crystal structures, and preliminary DNA-binding studies of four new DBTAA derivatives **8**–**11** (Scheme 1), designed on the basis of the structure of product **1**, which was found to be the most active compound in our previous evaluation[3,4] (Fig. 1).

The most significant structure modifications introduced to **8**–**11**, as compared with **1**, can be outlined as follows:

Compound **8**—pyridiniumyl has been replaced by a more sterically demanding, essentially spherical, trimethylammonium group. This may result in the exclusion of possible π–π interactions involving the pyridinium moiety, whilst the trimethylammonium group can act as a center of C_{sp3}–H proton donors. In this way, the pendant side chains become slightly shorter as compared with **1**, and their charged ends bulkier.

Compound **9**—the introduction of four methyl substituents to *o*-phenylene moieties may sterically disfavor π–π stacking interactions involving the main flat π-core of the macrocycle. It may therefore act against intercalative binding to DNA as well as against self-stacking of DBTAA moieties. Such reasoning appears to be consistent with the results reported earlier for the derivatives of porphyrin.[5,6] Some electron-donating influence of methyl groups on the π electron system should be also considered, as is shown by the UV–vis spectra.

Compounds **10** and **11**—incorporation of an *o*-substituted benzoyl moiety as a spacer between the flexible part of the substituents and the macrocyclic rings. As is shown by the crystal structure of **10** (vide infra) and of other derivatives previously reported,[7] the

* Corresponding author. Tel.: +48 12 6632294; fax: +48 12 6340515.
E-mail address: jeilmes@chemia.uj.edu.pl (J. Eilmes).

0040-4020/$ – see front matter © 2009 Elsevier Ltd. All rights reserved.
doi:10.1016/j.tet.2009.03.030

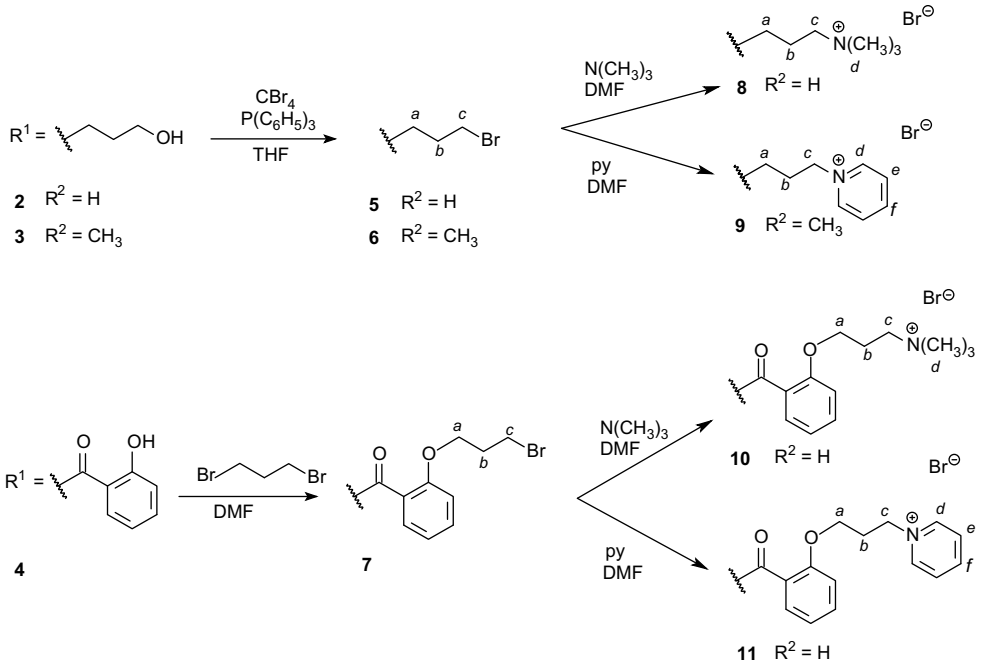

Scheme 1.

benzene rings of the benzoyl group are arranged almost perpendicularly to the planar macrocycle. This introduces remarkable rigidity and steric constraints in close vicinity to the macrocyclic core, thus also affecting the directional arrangement of the aliphatic part of the substituents. It is, therefore, apparent that the aliphatic chains terminated with trimethylammonium and pyridinium moieties have a tendency to adopt a more perpendicular orientation in respect to the main core, both above and below the ring. In consequence, a shielding of the aromatic surface from external access can be expected, preventing to some extent π–π stacking interactions with base pairs of DNA. Furthermore, assuming that the peripheral substituents may partially cover the flat π-plane of the macrocycle (as was found in a similar DBTAA derivative[7]), the dimensions and positive charges of the pyridinium and trimethylammonium groups located on the external part of these compact molecules may dictate the mode of interactions with DNA. The C═O part of the benzoyl groups also acts as an electron-withdrawing substituent and a source of an easily polarizable center of negative charge.

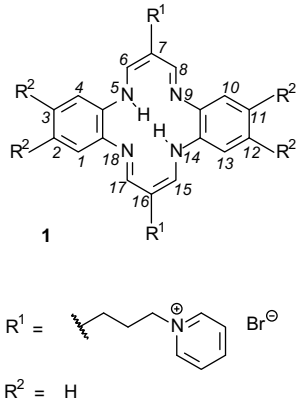

Figure 1. The most active compound in our previous evaluation.[3,4]

2. Results and discussion

2.1. Synthesis

Dicationic products **8** and **9** have been synthesized analogously to the procedure reported earlier,[3] starting from **2** and **3**.[8] Similarly, products **10** and **11**, equipped with *o*-substituted benzoyl spacers between the substituents and macrocyclic rings, have been prepared using **4**[9] and dibromopropane as an alkylating reagent.

All new products have been characterized by an elemental analysis, ^{1}H and ^{13}C NMR, ESI-MS and IR data. ^{1}H and ^{13}C NMR signals, with their assignments and other spectroscopic and analytical data, are collected in the Experimental section.

2.2. Crystallography

The structures of compounds **8** and **10** with the atomic numbering scheme are shown in Figures 2 and 3. Crystal data and structural refinement details are given in Table 1.

Compound **8** crystallizes in the $P2_1/c$ space group with one half of the tetraaza cation, one bromide anion, and one half of methanol solvent molecule in the asymmetric part of the unit cell. The methanol solvent molecule is disordered over two equal symmetry related sites with the carbon atom situated on the inversion center.

Compound **10** crystallizes in the $C2/c$ space group with one half of the tetraaza cation, one bromide anion, one methanol solvent molecule, and one water in the asymmetric part of the unit cell. The bromide anion is disordered over two positions (0.72 and 0.28), and water molecule has a partly site occupied factor of 0.28.

The central 14-membered ring of the macrocyclic cation in the structure of **8** has a planar conformation and lies across the center of inversion. The macrocyclic ring is, however, not ideally planar, and its distortion from planarity is up to 0.041(1) Å for the C9 atom. A conformation of an analogous tetraaza ring in the structure of **10** is distinctly deformed from planarity with a maximum deviation of 0.115(4) Å for the C7 atom.

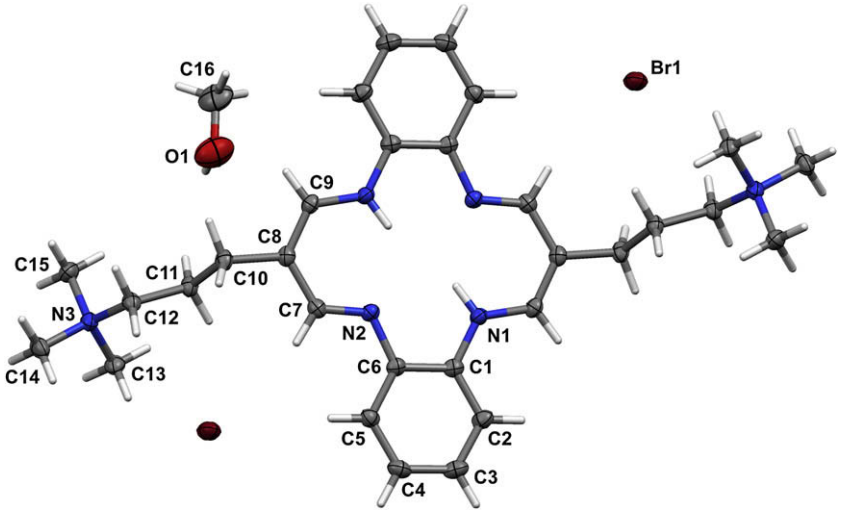

Figure 2. The molecular structure of **8** at 90 K, showing the atom-numbering scheme. Displacement ellipsoids for non-H atoms are drawn at the 50% probability level. Hydrogen bonds are shown as dashed lines. The unlabeled atoms are related to corresponding labeled atoms by the symmetry operation (−*x*+1, −*y*, −*z*+2).

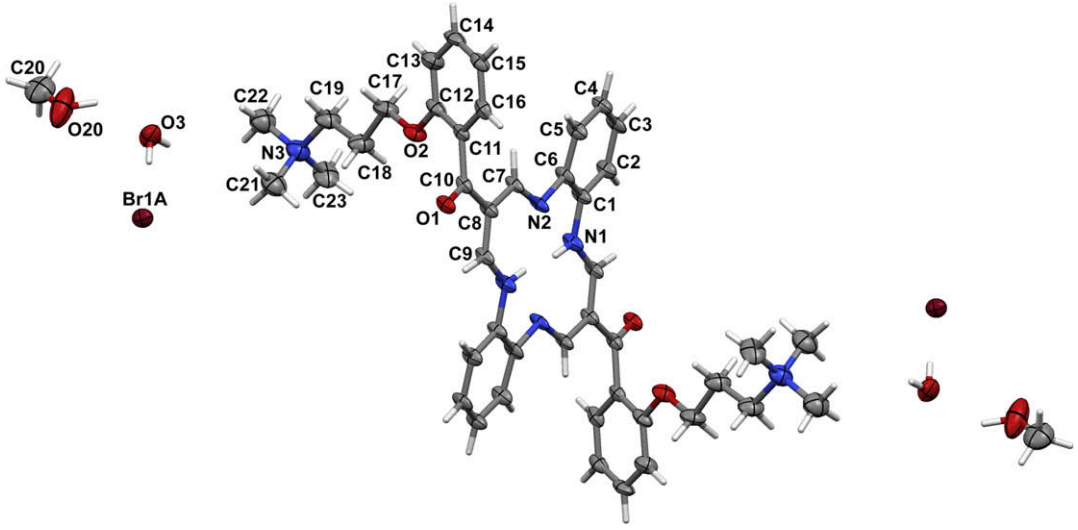

Figure 3. The molecular structure of **10** at 90 K, showing the atom-numbering scheme. Displacement ellipsoids for non-H atoms are drawn at the 50% probability level. Hydrogen bonds are shown as dashed lines. The unlabeled atoms are related to corresponding labeled atoms by the symmetry operation (−*x*, −*y*+1, −*z*+1).

The rings in both structures have two open aliphatic chains folded above and below the adjacent tetraaza macroring. The chains in both compounds adopt fully extended *anti*-periplanar conformation with torsion angles of C8–C10–C11–C12=165.64(14)° and C10–C11–C12–N3=172.09(13)° for **8**, and C12–O2–C17–C18=−171.5(5)°, O2–C17–C18–C19=177.2(5)°, and C17–C18–C19–N3=−175.1(5)° for **10**. The location of the chains with respect to the tetraaza ring in the compounds is visibly different. In **8**, the chains are stretched outside the central ring, whilst in **10** they extend above and below the ring (Figs. 4 and 8). Such an arrangement results in different interactions between molecules. The angle between the vector C8–N3 and the tetraaza ring plane is 145.7 and 90.0°, and the perpendicular distance between the N3 atom and the plane is 2.60 and 7.31 Å, for **8** and **10**, respectively. However, calculated dihedral angles defined between the mean plane of the aliphatic chain (defined on C10, C11, C12, N3, and C14 atoms for **8**, and on C17, C18, C19, N3, and C22 atoms for **10**) and the 14-membered macrocyclic tetraaza ring are identical for both structures, at approx. 83°. These values are similar to those found in two other dibenzotetraaza[14]annulene dibromide compounds.

The bromide anion in **8** is hydrogen bonded to the methanol molecule, as well as involved in six C–H···Br contacts (Fig. 5, Table 3). There is no evidence of significant π···π contacts between molecules (Fig. 6).

The shortest observed intermolecular contacts in **8** are C10–H10A···[C1–N1]$_{mid\text{-}point}$=2.705, C15–H15A···[C1–N1]$_{mid\text{-}point}$=2.879, C14–H14C···[C5–C6]$_{mid\text{-}point}$=2.699, and H12···[C7–N2]$_{mid\text{-}point}$=2.801 Å (Fig. 5). These may be classified as moderately strong C_{sp3}–H···π interactions since the H···mid-point distances are well below the 3.14 Å limit, which is considered as an attractive interaction.[10]

For compound **10**, a very rapid evaporation of the hydrating water in ambient temperature, causing decay of the crystal was observed. In consequence of this, the formal site occupancy factor for water is 0.72. This results in two positions of disordered bromine anion of 0.72 and 0.28, where the first one is hydrogen bonded to the partly present water molecule. The bromide anion is also involved in a hydrogen bond with the methanol molecule.

Similarly to **8**, the anions are in cooperative weak Br···H–C contacts with methyl and methylene groups. They stabilize their positions inside the channel together with hydrogen-bonded water and methanol solvent molecules (Fig. 7).

Table 1
Crystal data and structural refinement details for **8** and **10**

	8	**10**
Empirical formula	$C_{30}H_{44}N_6^{2+}\cdot 2Br^-\cdot CH_4O$	$C_{44}H_{54}N_6O_4^{2+}\cdot 2Br^-\cdot 2CH_4O\cdot 1.44H_2O$
Formula weight	680.55	978.74
Crystal system	Monoclinic	Monoclinic
Space group	$P2_1/c$	$C2/c$
a (Å)	12.4375(2)	36.009(4)
b (Å)	12.8276(2)	11.2827(13)
c (Å)	10.7040(2)	11.6343(13)
β (°)	106.180(1)	91.965(4)
V (Å^3), Z	1640.11(5), 2	4724.0(9), 4
d_{calcd} (g/cm^3)	1.378	1.376
F(000)	708	2042
Temperature (K)	90	90
Radiation type, wavelength (Å)	Cu Kα, 1.54178	Mo Kα, 0.71073
μ (mm^{-1})	3.385	1.772
θ range (°)	3.70–69.96	2.48–24.80
Limiting indices, h, k, l	$-15\rightarrow 15$, $-15\rightarrow 15$, $-11\rightarrow 12$	$-42\rightarrow 42$, $-13\rightarrow 13$, $-13\rightarrow 13$
Reflections collected	18,098	54,131
Unique reflections	3078 [R_{int}=0.018]	3967 [R_{int}=0.050]
Completeness to θ=70.0°	99.0%	97.5%
Data/restraints/parameters	3078/0/188	3967/0/298
Goodness-of-fit on F^2	1.068	1.164
Final R indices [$I>2\sigma(I)$]	R=0.0243, wR^2=0.0639	R=0.0677, wR^2=0.1587
Final R indices [all data]	R=0.0245, wR^2=0.0640	R=0.0716, wR^2=0.1600
Largest diff. peak and hole (e Å^{-3})	0.649, −0.355	0.557, −0.548

Compound **8**: weight=$1/[\sigma^2(F_0^2)+(0.0307P)^2+1.196P]$ where $P=(\max(F_0^2, 0)+2F_c^2)/3$. Compound **10**: weight=$1/[\sigma^2(F_0^2)+(0.0319P)^2+47.971P]$ where $P=(\max(F_0^2, 0)+2F_c^2)/3$.

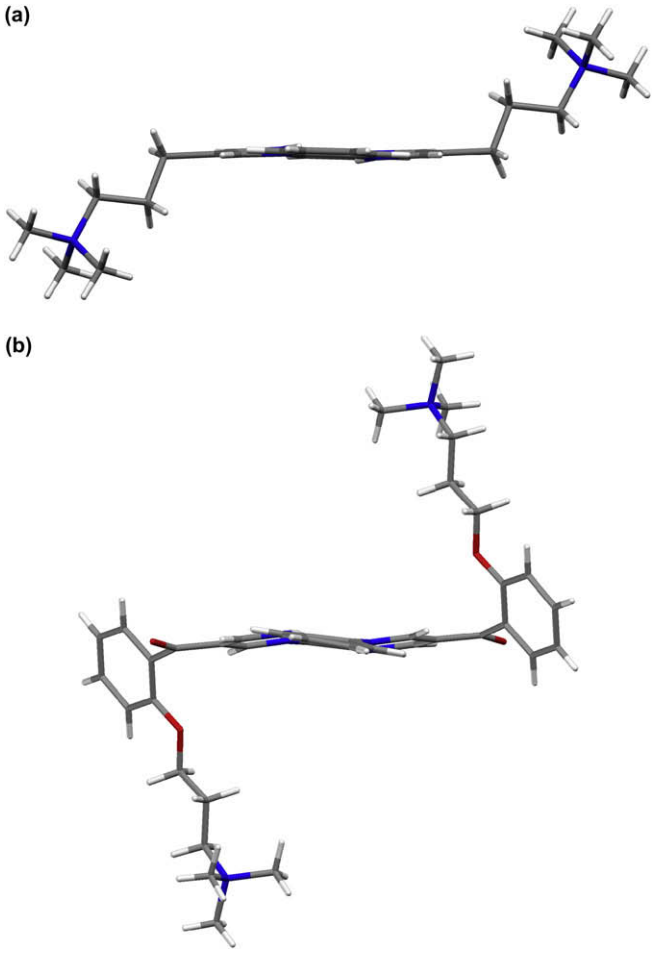

Figure 4. A view of the main molecules of **8** (a) and **10** (b) showing a different orientation of the aliphatic chain in respect to the central tetraaza ring.

2.3. Interactions of 8, 9, 10, and 11 with *calf thymus* (*ct*) DNA in aqueous medium

Compounds **8**–**11** are moderately soluble in the buffer system used (about $c=1\times10^{-3}$ mol dm^{-3} at pH=7, sodium cacodylate buffer, I=0.05 mol dm^{-3}). Buffered aqueous solutions of the studied compounds were stable for many days at room temperature. The changes of the UV–vis spectra on increasing temperature to 85 °C were negligible and the reproducibility of UV–vis spectra upon cooling back to 25 °C was excellent. The absorbencies of buffered aqueous solutions of the studied compounds are proportional to their concentrations up to $c=3$–4×10^{-5} mol dm^{-3}. Aforementioned data indicate that the studied compounds do not aggregate by intermolecular stacking at the experimental conditions used.

Comparison of the UV–vis spectra and corresponding molar extinction coefficients (ε) (Table 4, Fig. 9) revealed that two well resolved maxima of **8**, **9** in visible range ($\lambda>350$ nm), in the case of **10**, **11** merged into one significantly blue-shifted maximum accompanied with weak shoulder at about λ=400 nm. Such differences could be attributed to the significant impact of electron-withdrawing properties of carbonyl-containing substituents and nonplanar arrangement of benzoyl rings with respect to the macrocyclic ring.

Buffered (sodium cacodylate buffer, I=0.05 mol dm^{-3}, pH=7) aqueous solutions of **8**, **9** at $c=1\times10^{-5}$ mol dm^{-3} did not exhibit any fluorescence even at the highest sensitivity of the instrument, while at same conditions **10**, **11** showed only very weak fluorescence emission at λ=625 nm. Due to the strong inner filter effects it was not possible to perform experiments at higher concentrations.

The addition of *calf thymus* (*ct*) DNA yielded strong bathochromic and hypochromic effects in the UV–vis spectra of all studied compounds. Only in the UV–vis titration of **8**, isosbestic points are observed at $\lambda>300$ nm, pointing to the formation of one dominant type of complex (Fig. 10). Clear deviations from the isosbestic points observed for **9**–**11** as well as changes in opposite

Table 2
Selected geometric parameters (Å, °)

Compound **8**		Compound **10**	
N1–C1	1.394(2)	N1–C1	1.401(6)
N1–C9^{i}	1.357(2)	N1^{ii}–C9	1.317(6)
N2–C6	1.419(2)	N2–C6	1.422(5)
N2–C7	1.301(2)	N2–C7	1.296(6)
N3–C12	1.515(2)	N3–C19	1.510(7)
N3–C13	1.499(2)	N3–C21	1.479(8)
N3–C14	1.499(2)	N3–C22	1.506(8)
N3–C15	1.498(2)	N3–C23	1.503(8)
N1–C1–C2	122.82(14)	N1–C1–C2	122.2(4)
N1–C1–C6	117.42(14)	N1–C1–C6	118.0(4)
N1^{i}–C9–C8	124.45(14)	N1^{iii}–C9–C8	124.4(4)
N2–C6–C1	115.72(14)	N2–C6–C1	117.0(4)
N2–C6–C5	125.72(14)	N2–C6–C5	124.2(4)
N2–C7–C8	124.74(15)	N2–C7–C8	123.3(4)
N3–C12–C11	114.74(13)	N3–C19–C18	114.4(4)
C1–N1–C9^{i}	126.48(13)	C1–N1–C9^{iii}	127.0(4)
C6–N2–C7	119.55(13)	C6–N2–C7	117.9(4)
C12–N3–C13	111.23(12)	C19–N3–C21	111.3(5)
C12–N3–C14	108.49(13)	C19–N3–C22	107.2(4)
C12–N3–C15	110.37(13)	C19–N3–C23	110.7(5)
C13–N3–C14	108.44(13)	C21–N3–C22	108.1(5)
C13–N3–C15	109.54(13)	C21–N3–C23	110.4(5)
C14–N3–C15	108.72(13)	C22–N3–C23	109.0(5)

Symmetry codes: (i) $-x+1, -y, -z+2$; (ii) $-x, -y+1, -z$; (iii) $-x, -y+1, -z+1$.

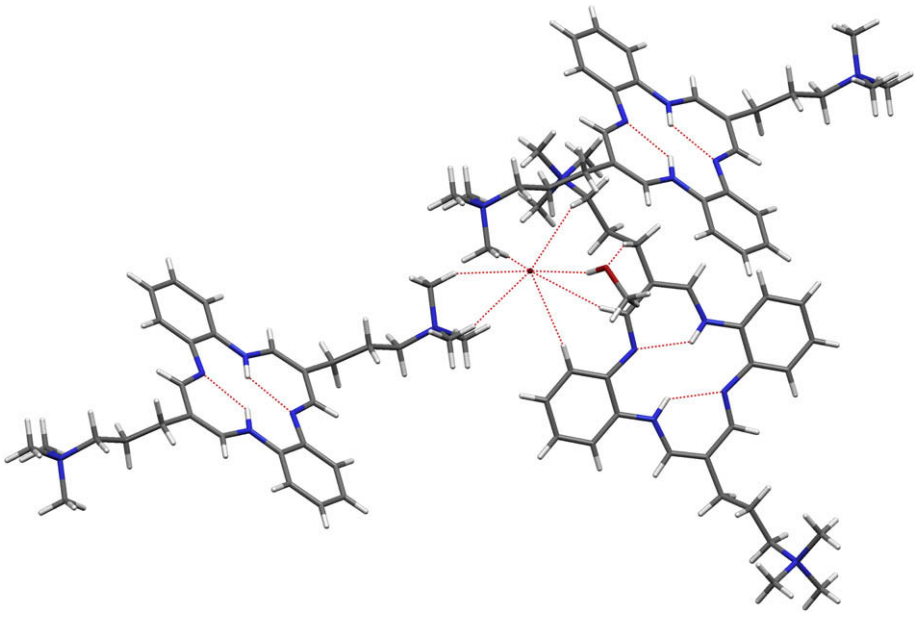

Figure 5. The intramolecular N–H···N and intermolecular C–H···Br and C–H···O contacts in **8**, shown as dashed lines.

directions with the breakpoint at about r=0.2 (only for **10** and **11**, Fig. 11) strongly supported co-existence of various types of complexes of **9**–**11** with (*ct*)-DNA in conditions close to the equimolar compound/DNA ratio. Therefore, binding constants K_s and ratios $n_{[\text{bound compound}]/[ct\text{-DNA}]}$ obtained for **9**, **10** by processing of UV–vis titration data according to Scatchard equation[11] (Table 5) can be considered only as the cumulative values describing various co-existing complexes.

In thermal denaturation experiments, addition of any of studied compounds stabilized the (*ct*)-DNA double helix (Table 5). Moreover, at different ratios $r_{[\text{compound}]/[ct\text{-DNA}]}$=0.1; 0.2; 0.3 strongly nonlinear dependence of ΔT_m values on the ratio r was observed, suggesting saturation of dominant binding sites at about r=0.25.

As an alternative method for estimation of the affinity toward DNA, at least as a comparison of ability of studied molecules to compete for binding with classical intercalator already bound to DNA,[12] we have performed ethidium bromide (**EB**) displacement assays (Fig. 12).

The obtained IC_{50} values suggest that the affinity of **8** and **9** toward (*ct*)-DNA is comparable to the affinity of **EB**, while **10** and **11** bind somewhat stronger than **EB**. This finding is in good agreement with the calculated binding constants from UV–vis titration, taking into account that binding constant of **EB** toward *ct*-DNA at the same experimental conditions is log K_s=6.[13]

To summarize, high binding constants and strong stabilization effects on a double helix of (*ct*)-DNA (Table 2), as well as the IC_{50} values determined in ethidium bromide displacement assays point to strong interactions of compounds **8**–**11** with (*ct*)-DNA. Moreover, pronounced hypochromic and bathochromic effects in the UV–vis

Table 3
Close contacts of hydrogen bond type in **8** and **10** [Å, °]

D–H···A	D–H	H···A	D···A	D–H···A
8				
N1–H1···N2$^{-x+1,\ -y,\ -z+2}$	0.88	2.11	2.775(2)	132
O1–H10···Br1$^{x,\ -y+1/2,\ z+1/2}$	0.84	2.68	3.501(5)	165
C10–H10B···O1$^{x,\ -y+1/2,\ z-1/2}$	0.99	2.64	3.580(4)	159
C5–H5···Br1	0.95	2.96	3.9050(17)	172
C7–H7···Br1	0.95	3.02	3.9501(16)	166
C12–H12A···Br1$^{x,\ -y+1/2,\ z+1/2}$	0.99	2.90	3.6888(17)	137
C13–H13C···Br1$^{-x+2,\ y+1/2,\ -z+3/2}$	0.98	2.90	3.7985(17)	154
C15–H15B···Br1$^{-x+2,\ y+1/2,\ -z+3/2}$	0.98	2.87	3.779(2)	154
C15–H15C···Br1$^{x,\ -y+1/2,\ z+1/2}$	0.98	2.95	3.853(2)	153
10				
N1–H1···N2$^{-x,\ -y+1,\ -z+1}$	0.88	2.07	2.727(5)	131
O3–H31···Br1A$^{-x+1/2,\ -y+1/2,\ -z}$	0.84	2.43	3.234(5)	161
O3–H32···Br1A	0.84	2.48	3.322(6)	176
O20–H20···O3	0.84	1.94	2.727(8)	155
C2–H2···O1$^{x,\ y+1,\ z}$	0.95	2.31	3.240(6)	167
C9–H9···O1$^{-x,\ -y,\ -z+1}$	0.95	2.59	3.533(6)	172
C16–H16···O1$^{-x,\ y,\ -z+3/2}$	0.95	2.45	3.394(6)	169
C19–H19A···Br1A$^{-x+1/2,\ -y-1/2,\ -z+1/2}$	0.99	2.69	3.632(7)	160
C22–H22A···Br1A	0.98	2.96	3.867(6)	155
C22–H22C···Br1A$^{x,\ -y+1,\ z+1/2}$	0.98	2.99	3.941(7)	164
C22–H22C···Br1B$^{x,\ -y+1,\ z+1/2}$	0.98	2.82	3.701(9)	151
C22–H22A···Br1B	0.98	3.01	3.935(8)	158
C23–H23C···Br1B	0.98	2.90	3.768(9)	148

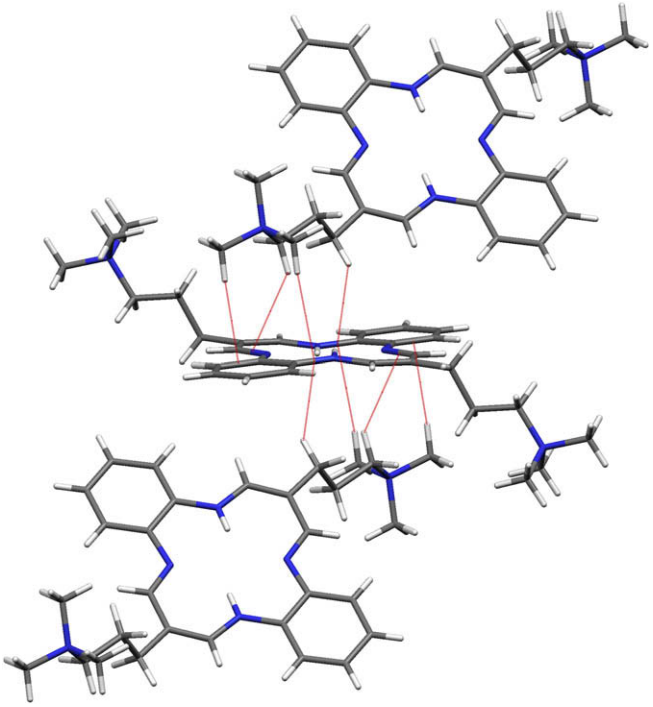

Figure 6. A mutual orientation of adjacent macrocyclic cations of **8** with C_{sp3}–H···π interactions indicated as dotted lines.

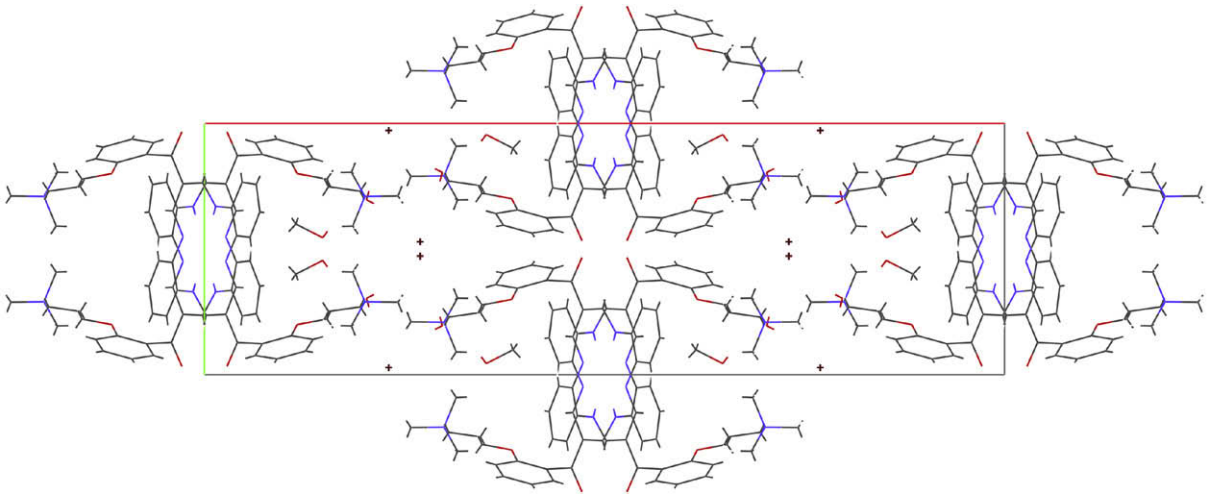

Figure 7. The channels in **10** running along the *c* axis with bromide anions located inside.

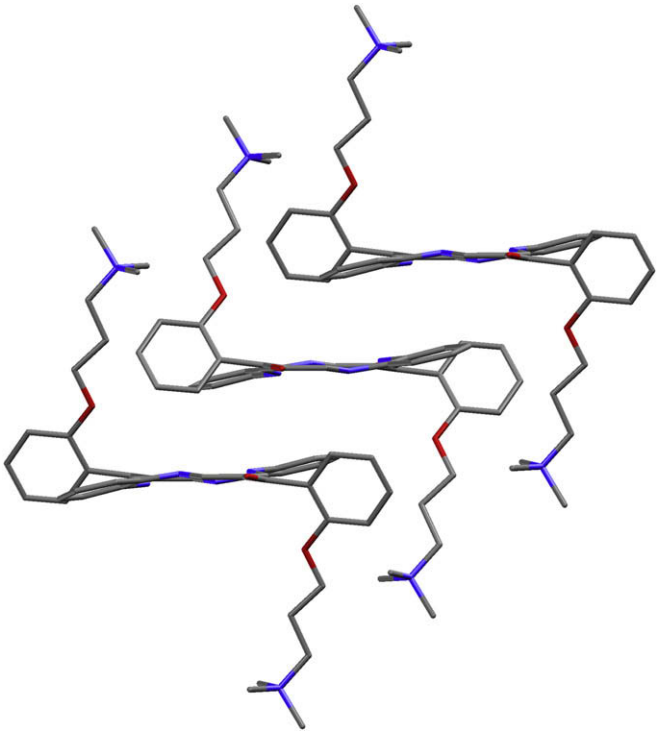

Figure 8. The main molecules of **10** interacting with each other via π···π stacking of parallel tetraaza ring layers with a distance of ca. 3 Å.

Table 4
Electronic absorption data of **8**–**11**[a]

	λ_{max}/nm	$\varepsilon\times10^3$/dm^3 mol^{-1} cm^{-1}
8	265	28.76
	377	40.32
	424	14.36
9	264	35.17
	385	39.58
	438	16.93
10	246	19.62
	344	47.61
11	257	27.32
	346	47.73

[a] Sodium cacodylate buffer, I=0.05 mol dm^{-3}, pH=7.

spectra of **8**–**11** upon titration with (*ct*)-DNA are most likely due to intensive aromatic stacking interactions involving molecules of **8**–**11** and DNA base pairs (intercalation) or to agglomeration of molecules along the DNA (groove binding). In addition, UV–vis titrations indicate that only **8** binds to DNA in one dominant binding mode, whereas **9**–**11** can be seen to form various different types of complexes with (*ct*)-DNA, although these cannot be precisely determined.

3. Conclusions

In order to fine tune the DNA-binding properties and the biological activity of dibenzotetraaza[14]annulenes, four new water-soluble derivatives have been designed and synthesized based on the structure of the most active compound from the previous evaluation. The new products **8**–**11** are characterized by 3-(*N*,*N*,*N*-trimethylammonium)-propyl and 3-(*N*-pyridinium-1-yl)propyl *meso* substituents and by different degrees of rigidity and steric constraints in the close vicinity of the planar macrocyclic ring.

Comparison of the X-ray structures of representative compounds **8** and **10** showed that the incorporation of rigid and relatively bulky *o*-benzoyl spacers into the peripheral substituents significantly influenced the spatial arrangement and directionality of the pendant side chains. Thus, the molecules of **10** appeared to have a nearly perpendicular orientation of trimethylammonium-propyl substituents in respect to the tetraaza plane (Figs. 4b and 8),

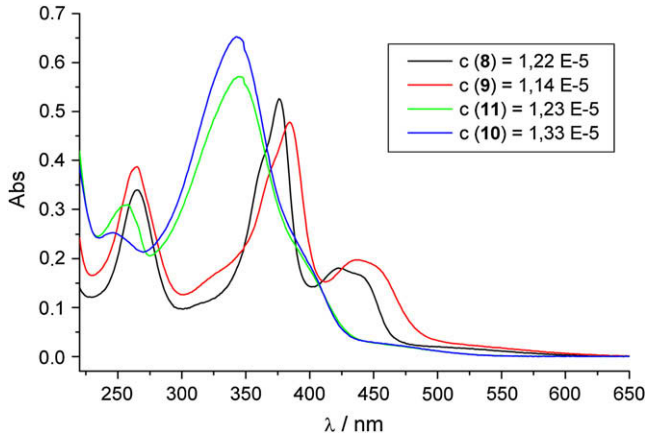

Figure 9. UV–vis spectra of **8**–**11** at c=1.1–1.3×10^{-5} mol dm^{-3}; pH=7, sodium cacodylate buffer, I=0.05 mol dm^{-3}.

whereas molecules of **8** adopted a more extended planar conformation, with the side chains stretched outside the molecule and with the central π-plane well exposed for external access (Fig. 4).

Spectrophotometric UV–vis titration with Scatchard analysis, thermal denaturation experiments, and ethidium bromide displacement assays showed strong mixed-mode interactions of **9**–**11** with (*ct*)-DNA and suggested only one dominant binding mode for compound **8**.

Judging solely from the molecular structures, it can be presumed that, from among **8**–**11**, compound **8** might be the best candidate for easy insertion and stacking between base pairs of double-helical DNA (intercalation). Being equipped with flexible aliphatic side chains, it therefore has an unhindered macrocyclic center that is well exposed, allowing for efficient π–π stacking. In contrast to **8**, compounds **9**–**11** bear bulky, rigid, and polar groups, located in close vicinity to the macrocyclic core. In view of the crystal structure of **10** and of other derivatives reported previously,[7] it may be posited that, in the case of compounds **9**–**11**, peripheral substituents sterically prevent intercalation to some extent and that they presumably render the molecules well suited to strong binding in the DNA grooves. As a consequence, mixed-mode interactions might be observed for **9**–**11**, as well as a somewhat higher affinity to DNA, as compared with **8**.

However, in order for the experimental results reported here to be correlated clearly with the structural details of **8**–**11**, more extensive and detailed investigations are necessary. Additional encouragement to further our study of products **8**–**11** is provided by the promising biological activity previously reported in regard to their closely related analogues.[4]

4. Experimental

4.1. General

Macrocyclic substrates **2**–**4** and **5** were prepared by the procedures described earlier.[3,8,9]

Other chemicals (tetrabromomethane, 1,3-dibromopropane, triphenylphosphine, triethylamine) were purchased from commercial sources (Sigma–Aldrich, Fluka) and were used as received. Solvents were dried using standard methods and were freshly distilled before use. Elemental analyses were performed on an Euro-EA (EuroVector) microanalyzer. ^{1}H and ^{13}C NMR were run on a Bruker AMX (500 MHz) and a Mercury Varian (300 MHz) spectrometers. Chemical shifts (δ) are expressed in parts per million and *J* values in hertz. Signal multiplicities are denoted as s (singlet), d (doublet), t (triplet), q (quartet), and m (multiplet). ESI mass spectra were taken on a Bruker Esquire 3000 spectrometer. The IR spectra were recorded in KBr with a Bruker IFS 48 spectrophotometer. Melting points were measured with use of a Boethius apparatus and were uncorrected.

4.2. Syntheses

*4.2.1. 7,16-Bis(3-bromopropyl)-2,3,11,12-tetramethyl-5,14-dihydrodibenzo[b,i][1,4,8,11]tetraazacyclotetradecine (**6**)*

Prepared analogous to **5**,[3] starting from **3** (0.2 g, 0.43 mmol), tetrabromomethane (0.57 g, 1.7 mmol), and triphenylphosphine (1.05 g, 4 mmol). Deep-red crystals, yield 0.15 g (75%), mp 248–249 °C (decomposition). ^{1}H NMR (500 MHz; $CDCl_3$+C_6D_6; 50 °C; δ ppm): 1.75 (m, 4H, H^b), 2.07 (s, 12H, CH_3), 2.17 (t, *J*=7.3 Hz, 4H, H^a), 3,17 (t, *J*=6.4 Hz, 4H, H^c), 6.75 (s, 4H, $H^{1,4}$, $H^{10,13}$), 7.49 (s, 4H, =CHN), 13.94 (br s, 2H, NH); ^{13}C NMR (125 MHz; $CDCl_3$+C_6D_6; 50 °C; δ ppm): 19.43 (CH_3), 31.38, 32.75, 35.05 (C^a, C^b, C^c), 105.88 ($C^{7,16}$), 114.96 ($C^{1,4}$, $C^{10,13}$), 132.47 ($C^{2,3}$, $C^{11,12}$), 136.06 ($C^{4a,18a}$, $C^{9a,13a}$), 146.45 (C=N); IR (KBr) ν_{max} (cm^{-1}): 3452 (s, N–H), 3054 (s,=C–H); 2959, 2917, 2851 (s, C–H), 1642, 1607 (s, C=C), 1549 (br, N–H, C–N), 1514, 1450 (br, C–H), 1422, 1402, 1347, 1306, 1272, 1254, 1245, 1192, 1001; ESI-MS (*m*/*z*): 584.2 ($C_{28}H_{34}Br_2N_4$+H^+). Anal. Calcd for $C_{28}H_{34}Br_2N_4$: C, 57.35; H, 5.84; N, 9.55. Found: C, 57.31; H, 6.08; N, 9.46%.

*4.2.2. 7,16-Bis[2-(3-bromopropoxy)benzoyl]-5,14-dihydrodibenzo[b,i][1,4,8,11]tetraazacyclotetradecine (**7**)*

A reaction mixture consisting of **4** (0.87 g, 1.65 mmol), anhydrous potassium carbonate (0.9 g, 6.6 mmol), 1,3-dibromopropane (2 mL, 19.8 mmol), and anhydrous dimethylformamide (100 mL) was stirred magnetically at room temperature for 48 h. A solid material was filtered off, filtrate was diluted with water to precipitate the product, and left in a refrigerator for 24 h. A crude product was filtered off, washed with ethanol, and dried under vacuum. It was dissolved in chloroform (12 mL) introduced on a column of silicagel and chromatographed using toluene/acetone (40:1) as eluent. The main orange fraction was collected, concentrated to about 90 mL, diluted with *n*-hexane (10 mL), and left aside for 24 h. Orange microcrystalline product was collected by filtration, washed with *n*-hexane, and dried under vacuum. Yield 0.9 g (70%), mp 225–227 °C. ^{1}H NMR (300 MHz; $CDCl_3$; δ ppm): 2.21 (m, 4H, H^b), 3.45 (t, *J*=6.2 Hz, 4H, H^c), 4.147 (t, *J*=5.8 Hz, 4H, H^a), 7.01–7.19 (m, 12H, H^{1-4}, H^{10-13}, *o*-C_6H_4'), 7.37 (dd, *J*=1.7, 7.5 Hz, 2H, *o*-C_6H_4'), 7.45 (ddd, *J*=8.2, *J*=7.5, *J*=1.7 Hz, 2H, *o*-C_6H_4'), 8.58 (br, 4H, =CHN), 14.40 (br, 2H, NH); ^{13}C NMR (75 MHz; $CDCl_3$; δ ppm): 30.13 (C^b), 32.24 (C^c), 66.17(C^a), 110.82, 112.78, 115.68, 121.55, 126.66, 129.44, 129.73, 131.42, 137.26, 155.59 (*o*-C_6H_4, *o*-C_6H_4', C=N), 192.95 (C=O); IR (KBr) ν_{max} (cm^{-1}): 3454 (s, N–H), 3066 (s, =C–H), 2922, 2879 (s, C–H); 1616, 1564, 1496, 1484, 1448, 1420, 1403; ESI-MS (*m*/*z*): 771.1

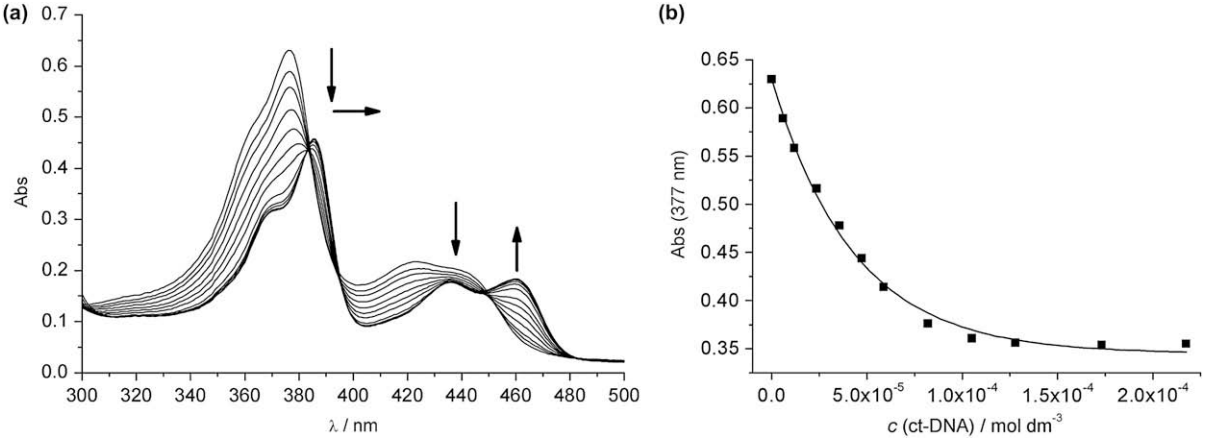

Figure 10. (a) Changes in UV–vis spectrum of **8** (c=1.53×10^{-5} mol dm^{-3}) upon titration with *ct*-DNA; (b) dependence of absorbance of **8** at λ_{max}=377 nm on c(*ct*-DNA), at pH=7, sodium cacodylate buffer, I=0.05 mol dm^{-3}.

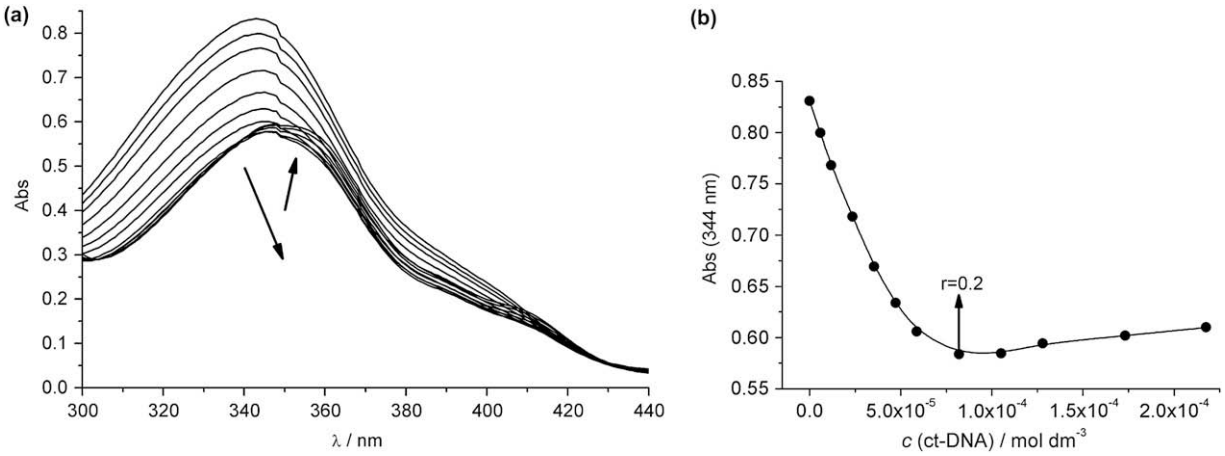

Figure 11. (a) Changes in UV–vis spectrum of **10** (c=1.66×10^{-5} mol dm^{-3}) upon titration with *ct*-DNA; (b) dependence of absorbance of **10** at λ_{max}=344 nm on c(*ct*-DNA), at pH=7, sodium cacodylate buffer, I=0.05 mol dm^{-3}.

($C_{38}H_{34}Br_2N_4O_4$+H^+). Anal. Calcd for $C_{38}H_{34}$ $Br_2N_4O_4$: C, 59.24; H, 4.45; N, 7.27. Found: C, 59.61; H, 4.62; N, 7.04%.

4.2.3. 7,16-Bis[3-(N,N,N-trimethylammonium)propyl]-5,14-dihydrodibenzo[b,i][1,4,8,11]tetraazacyclotetradecine dibromide (**8**)

To a cold solution of **5** (0.15 g, 0.19 mmol) in anhydrous DMF (50 mL), cooled to −10 °C, trimethylamine (2 mL, 21 mmol) was added. The reaction mixture was stirred at 45 °C, under argon for 48 h. The solution was concentrated to a small volume and diluted with diethyl ether to afford crystalline product. The product can be additionally purified on a column of basic aluminum oxide (Fluka) using methylene chloride/methanol (90:1) as eluent. Red crystals, yield 0.125 g (67%), mp>260 °C. Crystals suitable for X-ray measurements were grown by slow diffusion of *tert*-butyl methyl ether into a solution of **8** in methanol. ^{1}H NMR (300 MHz; DMSO-d_6; δ ppm): 1.92 (m, 4H, H^b), 2.27 (t, J=7.4 Hz, 4H, H^a), 3.09 (s, 18H, H^d), 3.35 (t, J=5.2 Hz, 4H, H^c), 6.93 (dd, J=6.0, 3.2 Hz, 4H, H^{2,3}, H^{11,12}), 7.32 (dd, J=6.0, 3.2 Hz, 4H, H^{1,4}, H^{10,13}), 7.90 (d, J=5.9 Hz, 4H, =CHN), 13.57 (t, J=5.9 Hz, 2H, NH); ^{13}C NMR (75 MHz; DMSO-d_6; δ ppm): 24.64, 28.77 (C^a, C^b), 52.19 (C^d), 64.78 (C^c), 106.39 (C^{7,16}), 113.93 (C^{1,4}, C^{10,13}), 124.19 (C^{2,3}, C^{11,12}), 136.72 (C^{4a,18a}, C^{9a,13a}), 147.73 (C=N); IR (KBr) ν_{max} (cm^{-1}): 3475, 3403 (s, N–H, O–H), 3064, 3031, 3005 (s, =C–H); 2944, 2918, 2871, 2853 (s, C–H), 1650, 1594 (s, C=C), 1552 (br, N–H, C–N), 1482; 1455 (br, C–H), 1424, 1401, 1356, 1314, 1293, 1219, 1158, 1004, ESI-MS (m/z): 244.5 ($C_{30}H_{44}N_6^{2+}$/2), Anal. Calcd for $C_{30}H_{44}Br_2N_6$:C, 55.56; H, 6.84; N, 12.96%. Found: C, 55.42; H, 6.65; N, 12.99%.

Table 5
Changes of **8**–**11** UV–vis spectra upon titration with (*ct*)-DNA, binding constants (log K_s) and ratios $n_{[bound\ compound]/[ct\text{-}DNA]}$ calculated from the UV–vis titrations;[a] and thermal denaturation data (ΔT_m values/°C)[e] of (*ct*)-DNA upon addition of **8**–**11** (pH=7.0, sodium cacodylate buffer, I=0.05 mol dm^{-3})

	$\Delta\lambda_1$[b]/nm	$\Delta\lambda_2$[b]/nm	H[c]/%	log K_s	n[d]	ΔT_m[e]/°C
8	9	12	45	5.85	0.26	6.6
9	5	5	35	5.69	0.32	3.1
10	6	—	28	6.80	0.32	10.2
11	3	—	25	[f]>7	[f]	12.8

[a] Titration data were processed according to the Scatchard equation.[11]
[b] $\Delta\lambda$=λ(**8**, **9**, **10**, and **11**)−λ(complex); absorbance maxima λ_1=(**8**$_{\lambda 377nm}$, **9**$_{\lambda 385nm}$, **10**$_{\lambda 344nm}$, **11**$_{\lambda 346nm}$,), λ_2=(**8**$_{\lambda 424nm}$, **9**$_{\lambda 438nm}$).
[c] Hypochromic effect calculated by Scatchard for **8**, **9**, **10**, and **11**; H=((Abs(**8**, **9**, **10**, and **11**)−Abs(complex))/Abs(**8**, **9**, **10**, and **11**))×100.
[d] Accuracy of n: ±10–30%, consequently log K_s values vary in the same order of magnitude.
[e] Error in ΔT_m: ±0.5 °C; $r_{[compound]/[ct\text{-}DNA]}$=0.3.
[f] Change of **11** UV–vis spectrum was almost linearly dependent on the c(*ct*)-DNA up to r=0.16, followed by the abrupt end of titration.

4.2.4. 7,16-Bis[3-(N-pyridinium-1-yl)propyl]-2,3,11,12-tetramethyl-5,14-dihydrodibenzo[b,i][1,4,8,11]tetraazacyclotetradecine dibromide monohydrate (**9**)

A reaction mixture consisting of **6** (0.10 g, 0.17 mmol), pyridine (10 mL, 120 mmol), and DMF (10 mL) was stirred at 45 °C under argon for 24 h. The mixture was concentrated on a rotary evaporator to half volume, diluted with diethyl ether (50 mL), and left in a refrigerator to afford crystalline product. It was purified chromatographically (basic aluminum oxide, methylene chloride/methanol (90:1)). Deep-red crystals, yield 0.044 g (35%), mp 244 °C. ^{1}H NMR (300 MHz; DMSO-d_6; δ ppm): 2.19 (m, 16H, CH_3, H^b), 2.29 (t, J=6.4 Hz, 4H, H^a), 4.68 (t, J=7.1 Hz, 4H, H^c), 7.03 (s, 4H, H^{1,4}, H^{10,13}), 7.76 (d, J=5.9 Hz, 4H, =CHN), 8.16 (dd, J=6.7, 7.7 Hz, 4H, H^e), 8.60 (tt, J=7.8, 1.3 Hz, 2H, H^f), 9.17 (dd, J=6.7, 1.2 Hz, 4H, H^d), 13.65 (t, J=6.0 Hz, 2H, NH); ^{13}C NMR (75 MHz; DMSO-d_6; δ ppm): 18.97 (CH_3), 28.77, 32.91 (C^a, C^b), 60.48 (C^c), 105.65 (C^{7,16}), 114.61 (C^{1,4}, C^{10,13}), 127.86 (C^e), 131.91 (C^{2,3}, C^{11,12}), 134.35 (C^{4a,18a}, C^{9a,13a}), 144.71, 145.28 (C^d, C^f), 146.67 (C=N); IR (KBr) ν_{max} (cm^{-1}): 3369 (s, N–H, O–H), 3041 (s, =C–H), 2917, 2879, 2851 (s, C–H), 1638, 1606 (s,

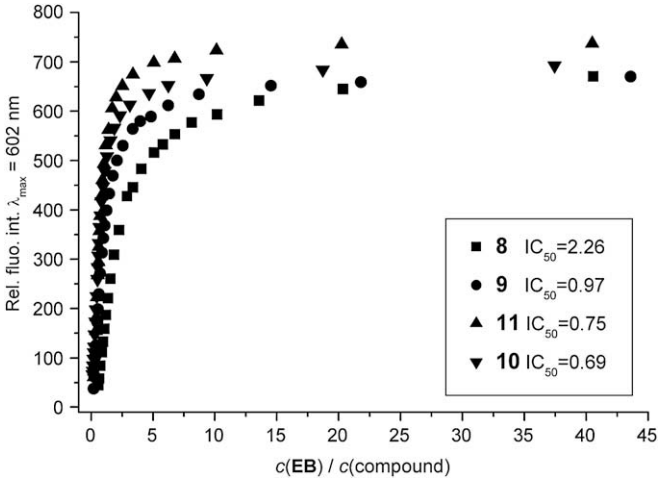

Figure 12. Ethidium bromide (**EB**) displacement assay: to *ct*-DNA solution (c=5×10^{-5} mol dm^{-3}), ethidium bromide (c=5×10^{-6} mol dm^{-3}) was added (r([**EB**]/[*ct*-DNA])=0.1), and quenching of the **EB**/DNA complex fluorescence emission (λ_{ex}=520 nm, λ_{em}=601 nm) was monitored as function of c(**EB**)/c(compound). The given IC_{50} values present the ratio c(**EB**)/c(compound)=[Int(**EB**/DNA)−Int(**EB**$_{free}$)]/2, where Int(**EB**/DNA) is fluorescence intensity of **EB**/DNA complex and Int(**EB**$_{free}$) is fluorescence intensity of the free ethidium bromide before DNA is added.

C=C), 1548 (br, N–H, C–N), 1516, 1486, 1447 (br, C–H), 1427, 1404, 1351, 1306, 1274, 1176.

ESI-MS (m/z): 291.7 ($C_{38}H_{44}N_6^{2+}/2$). Anal. Calcd for $C_{38}H_{44}Br_2N_6 \cdot H_2O$: C, 59.85; H, 6.08; N, 11.02. Found: C, 59.72; H, 6.09; N, 10.65%.

4.2.5. 7,16-Bis{2-[3-(N,N,N-trimethylammonium)propoxy]benzoyl}-5,14-dihydrodibenzo[b,i][1,4,8,11]tetraazacyclotetradecine dibromide dihydrate (**10**)

To a solution of **7** (0.20 g, 0.26 mmol) in anhydrous DMF (20 mL, cooled to −10 °C), trimethylamine (2 mL, 21 mmol) was added and the mixture was stirred at 45 °C, under argon for 24 h. The mixture was evaporated to dryness and the residue dissolved in a small quantity of methylene chloride was chromatographed on a column with basic aluminum oxide with use of methylene chloride/methanol (100:3) as eluent. The main fraction was collected, concentrated to a small volume, and diluted with *tert*-butyl methyl ether (50 mL). Crystalline product was filtered off, washed with *tert*-butyl methyl ether, and dried under vacuum. Deep-orange crystals, yield 0.12 g (52%), mp 243–244 °C. Crystals suitable for X-ray measurements were grown by slow diffusion of *n*-hexane into the solution of **10** in methylene chloride/methanol (1:1). ^{1}H NMR (300 MHz; d6-DMSO; δ ppm): 2.06 (m, 4H, H^b), 2.97 (s, 18H, H^d), 3.33 (m, 4H, H^c), 4.13 (t, J=5.9 Hz, 4H, H^a), 7.14–7.25 (m, 8H, H^{2,3}, H^{11,12}, o-C$_4$H$_6$′), 7.30 (dd, J=3.5, 6.2 Hz, H^{1,4}, H^{10,13}), 7.37 (dd, J=1.7, 7.5 Hz, 2H, o-C$_4$H$_6$′), 7.55 (m, 2H, o-C$_4$H$_6$′), 8.52 (d, J=6.5 Hz, 4H, =CHN), 14.29 (t, J=6.5 Hz, 2H, NH); ^{13}C NMR (75 MHz; DMSO-d_6; δ ppm): 22.49 (C^b), 52.03 (C^d), 62.76, 65.19 (C^a, C^c), 110.08 (C^{7,16}), 113.19, 115.52, 121.18, 126.89, 128.72, 129.10, 131.52, 136.16, 152.60, 154.84 (o-C$_6$H$_4$, o-C$_6$H$_4$′, C=N), 191.27 (C=O); IR (KBr) ν_{max} (cm^{-1}): 3426 (s, N–H, O–H), 3068, 3012 (s, =C–H), 2960 (s, C–H), 1647, 1591 (s, C=C), 1562 (br, N–H, C–N), 1489, 1444 (br, C–H), 1415, 1324, 1312, 1292, 1258, 1221, 1165, 1144, 1110, 1097, 1050, 1019; ESI-MS (m/z): 364.3 ($C_{44}H_{52}N_6O_4^{2+}/2$). Anal. Calcd for $C_{44}H_{52}Br_2N_6O_4 \cdot 2H_2O$: C, 57.15; H, 6.10; N, 9.09. Found: C, 57.24; H, 6.01; N, 9.16%.

4.2.6. 7,16-Bis{2-[3-(N-pyridinium-1-yl)propoxy]benzoyl}-5,14-dihydrodibenzo[b,i][1,4,8,11]tetraazacyclotetradecine dibromide dihydrate (**11**)

A reaction mixture consisting of **7** (0.2 g, 0.26 mmol), pyridine (10 mL, 120 mmol), and DMF (10 mL) was stirred at 45 °C under argon for 24 h. The solution was evaporated to dryness on a rotary evaporator. The solid residue dissolved in a small quantity of methylene chloride was chromatographed on a column of basic aluminum oxide using methylene chloride/methanol (100:5) as eluent. The main fraction was concentrated to a small volume and diluted with *tert*-butyl methyl ether to afford crystalline product. The product was filtered off, washed with *tert*-butyl methyl ether and dried under vacuum. Deep-orange crystals, yield 0.08 g (33%), mp 225–226 °C. ^{1}H NMR (300 MHz; d6-DMSO; δ ppm): 2.30 (m, 4H, H^b), 4.14 (t, J=5.8 Hz, 4H, H^a), 4.66 (t, J=6.7 Hz, 4H, H^c), 7.09–7.20 (m, 8H, H^{2,3}, H^{11,12}, o-C$_4$H$_6$′), 7.29 (dd, J=3.5, 6.0 Hz, H^{1,4}, H^{10,13}), 7.37 (dd, J=1.6, 7.5 Hz, 2H, o-C$_4$H$_6$′), 7.52 (m, 2H, o-C$_4$H$_6$′), 8.01 (m, 4H, H^e), 8.46 (d, J=6.5 Hz, 4H, =CHN), 8.60 (t, J=7.8 Hz, 2H, H^f), 9.17 (d, J=5.6 Hz, 4H, H^d), 14.23 (t, J=6.5 Hz, 2H, NH); ^{13}C NMR (75 MHz; DMSO-d_6; δ ppm): 29.98 (C^b), 58.16, 64.94 (C^a, C^c), 109.81 (C^{7,16}), 112.97, 115.53, 121.01, 126.86, 127.81, 128.49, 129.10, 131.47, 136.19, 144.59, 145.40, 152.60, 154.78 (o-C$_6$H$_4$, o-C$_6$H$_4$′, C=N, py), 191.17 (C=O); IR (KBr) ν_{max} (cm^{-1}): 3416 (s, N–H, O–H), 3052, 3031 (s, =C–H), 2961, 2934, 2886 (s, C–H), 1630, 1615, 1594 (s, C=C), 1563 (br, N–H, C–N), 1487, 1447 (br, C–H), 1401, 1323, 1290, 1265, 1248, 1170, 1096; 1048; ESI-MS (m/z): 384.3 ($C_{48}H_{44}N_6O_4^{2+}/2$). Anal. Calcd for: $C_{48}H_{44}Br_2N_6O_4 \cdot 2H_2O$: C, 59.76; H, 5.01; N, 8.71. Found: C, 59.98; H, 4.96; N, 8.69%.

4.3. Crystallography

Intensity data for the crystals of **8** and **10** were collected on a Bruker AXS Smart APEX-II CCD 3-circle diffractometer with MonoCap capillary and monochromated Cu Kα radiation (λ=1.54178 Å) (**8**) or Mo Kα radiation (λ=0.71973 Å), both at a temperature of 90 K. The data collection and data integration carried out with the SMART[14] and SAINT-PLUS[15] programs. Empirical absorption corrections were done using the SADABS program[16] The structure was solved by direct methods by using the SHELXS-97 program.[17] All non-hydrogen atoms were refined anisotropically by full-matrix least-squares based on F^2 using the SHELXL-97 program,[17] and the complete set of reflections. The final geometrical calculations were carried out with the PLATON program.[18] Figures were drawn using Mercury[19] program. The relevant crystal data and experimental details are summarized in Table 1.

All hydrogen atoms were placed geometrically with C–H=0.95–0.99, N–H=0.88, and O–H=0.84 Å, and included in the refinement as riding atoms with U_{iso}(H)=1.2 U$_{eq}$ (C,N) or 1.5 U$_{eq}$ (C$_{methyl}$,O).

4.4. UV–vis spectroscopy

The electronic absorption spectra were obtained on Varian Cary 100 Bio spectrometer and fluorescence spectra on the Varian Eclipse fluorimeter, all in quartz cuvettes (1 cm). The spectroscopic studies were performed in aqueous buffer solution (pH=7, sodium cacodylate buffer, I=0.05 mol dm^{-3}). Under the experimental conditions absorbance of **8**–**11** was proportional to their concentrations. The *calf thymus* (*ct*)-DNA was purchased from Aldrich, dissolved in sodium cacodylate buffer, I=0.05 mol dm^{-3}, pH=7, additionally sonicated and filtered through a 0.45 μm filter.[20,21] Polynucleotide concentration was determined spectroscopically[21] as the concentration of nucleotides. Spectroscopic titrations were performed by adding portions of polynucleotide solution into the solution of the studied compound. Obtained data were corrected for dilution. Titration data were processed by Scatchard equation.[11] Values for K_s and n given in Table 5 all have satisfactory correlation coefficients (>0.999). Thermal denaturation curves for DNA and its complexes with studied compounds were determined as previously described[21] by following the absorption change at 260 nm as a function of temperature. Absorbance of the ligands was subtracted from every curve, and the absorbance scale was normalized. The T_m values are the mid-points of the transition curves, determined from the maximum of the first derivative and checked graphically by the tangent method.[21] ΔT_m values were calculated subtracting T_m of the free nucleic acid from T_m of the complex. Every ΔT_m value reported here was the average of at least two measurements, the error in ΔT_m is ±0.5 °C.

Ethidium bromide (**EB**) displacement assay was done as follows: to *ct*-DNA solution (c=5×10^{-5} mol dm^{-3}), ethidium bromide (c=5×10^{-6} mol dm^{-3}) was added (r([**EB**]/[*ct*-DNA])=0.1), and quenching of the **EB**/DNA complex fluorescence emission (λ_{ex}=520 nm, λ_{em}=601 nm) was monitored as function of c(**EB**)/c(compound). The given IC$_{50}$ values present ratio c(**EB**)/c(compound)=[Int(**EB**/DNA)−Int(**EB**$_{free}$)]/2, where Int(**EB**/DNA) is fluorescence intensity of **EB**/DNA complex and Int(**EB**$_{free}$) is fluorescence intensity of the free ethidium bromide before DNA is added.

5. Supplementary data

Full details of crystallographic data for the structural analysis have been deposited with the Cambridge Crystallographic Data Centre, CCDC No. 711500 for compound **8** and No. 711501 for compound **10**. Copies of this information can be obtained free of charge via www.ccdc.cam.ac.uk/data_request/cif.

References and notes

1. (a) Johnson, D. S.; Boger, D. L. In *Comprehensive Supramolecular Chemistry*; Atwood, J. L., Davies, J. E. D., MacNicol, D. D., Vögtle, F., Eds.; Pergamon: Oxford, New York, NY, 1996; Vol. 4, Chapter 3, pp 73–176 and references cited therein; (b) *DNA and RNA Binders*; Demeunynck, M., Bailly, C., Wilson, W. D., Eds.; Wiley-VCH: Weinheim, 2003; (c) Martinez, R.; Chacon-Garcia, L. *Curr. Med. Chem.* **2005**, *12*, 127–151; (d) Zeglis, B. M.; Pierre, V. C.; Barton, J. K. *Chem. Commun.* **2007**, 4565–4579; (e) Hannon, M. J. *Chem. Soc. Rev.* **2007**, *36*, 280–295.
2. (a) McMillin, D. R.; Shelton, A. H.; Bejune, S. A.; Fanwick, P. E.; Wall, R. K. *Coord. Chem. Rev.* **2005**, *249*, 1451–1459; (b) McMillin, D. R.; McNett, K. M. *Chem. Rev.* **1998**, *98*, 1201–1220; (c) Pasternack, R. F.; Gibs, E. J.; Villafranca, J. J. *Biochemistry* **1983**, *22*, 2406–2414; (d) Fiel, R. J. *J. Biomol. Struct. Dyn.* **1989**, *6*, 1259–1274; (e) Fiel, R. J.; Howard, J. C.; Mark, E. H.; Datta-Gupta, N. *Nucleic Acids Res.* **1979**, *6*, 3093–3118.
3. Pawlica, D.; Radić Stojković, M.; Sieroń, L.; Piantanida, I.; Eilmes, J. *Tetrahedron* **2006**, *62*, 9156–9165.
4. Radić-Stojković, M.; Piantanida, I.; Kralj, M.; Marjanović, M.; Žinić, M.; Pawlica, D.; Eilmes, J. *Bioorg. Med. Chem.* **2007**, *15*, 1795–1801.
5. Marzilli, L. G.; Pethö, G.; Lin, M.; Kim, M. S. *J. Am. Chem. Soc.* **1992**, *114*, 7575–7577 and references cited therein.
6. Kano, K.; Fukuda, K.; Wakami, H.; Nishiyabu, R.; Pasternack, R. F. *J. Am. Chem. Soc.* **2000**, *122*, 7494–7502.
7. Grolik, J.; Dominiak, P. M.; Sieroń, L.; Woźniak, K.; Eilmes, J. *Tetrahedron* **2008**, *64*, 7796–7806.
8. Hanke, R.; Breitmaier, E. *Chem. Ber.* **1982**, 1657–1661.
9. Sigg, I.; Haas, G.; Winkler, T. *Helv. Chim. Acta* **1982**, *65*, 275–279.
10. Bond, A. D. *Chem. Commun.* **2002**, 1664–1665.
11. (a) Scatchard, G. *Ann. N.Y. Acad. Sci.* **1949**, *51*, 660–672; (b) McGhee, J. D.; von Hippel, P. H. *J. Mol. Biol.* **1976**, *103*, 679–684.
12. Boger, D. L.; Fink, B. E.; Brunette, S. R.; Tse, W. C.; Hedrick, M. P. *J. Am. Chem. Soc.* **2001**, *123*, 5878–5891.
13. Piantanida, I.; Palm, B. S.; Žinić, M.; Schneider, H.-J. *J. Chem. Soc., Perkin Trans. 2* **2001**, 1808–1816.
14. Bruker. *SMART for WNT/2000. Version 5.630*; Bruker AXS: Madison, WI, USA, 2002.
15. Bruker. *SAINT-Plus (Version 6.45)*; Bruker AXS: Madison, WI, USA, 2003.
16. Sheldrick, G. M. *SADABS, Program for Area Detector Adsorption Correction, v. 2.10*; Institute for Inorganic Chemistry, University of Göttingen: Germany, 2003.
17. Sheldrick, G. M. *Acta Crystallogr.* **2008**, *A64*, 112–122.
18. Spek, A. L. *J. Appl. Crystallogr.* **2003**, *36*, 7–13.
19. Macrae, C. F.; Edgington, P. R.; McCabe, P.; Pidcock, E.; Shields, G. P.; Taylor, R.; Towler, M.; van de Streek, J. *J. Appl. Crystallogr.* **2006**, *39*, 453–457.
20. Chaires, J. B.; Dattagupta, N.; Crothers, D. M. *Biochemistry* **1982**, *21*, 3933–3940.
21. Palm, B. S.; Piantanida, I.; Žinić, M.; Schneider, H. J. *J. Chem. Soc., Perkin Trans. 2* **2000**, 385–392.